Supplementary Materials: Atmospheric forcing and photo-acclimation of phytoplankton fall blooms in Hudson Bay

Lucas Barbedo[1,2,*], Simon Bélanger[1,*], Jennifer V. Lukovich[3], Paul G. Myers[4], Jean-Éric Tremblay[5,6]

[1]Université du Québec à Rimouski, Département de biologie, chimie et géographie, groupes BORÉAS et Québec-Océan, 300, allée des Ursulines, Rimouski, Québec G5L 3A1, Canada

[2]The University of Southern Mississippi, Division of Marine Science, School of Ocean Science and Engineering, Stennis Space Center, Mississippi 59529, USA

[3]University of Manitoba, Department of Environment and Geography, Center for Earth Observation Science, Winnipeg, Manitoba, Canada

[4]University of Alberta, Department of Earth and Atmospheric Sciences, Edmonton, Alberta, Canada

[5]Takuvik Joint International Laboratory, Laval University (Canada), CNRS, FR

[6]Département de biologie et Québec-Océan, Université Laval, Québec, CA

[*] lucasbarbedo@gmail.com, simon_belanger@uqar.ca

Text S1. Evaluation of chlorophyll-*a* concentration ocean color satellite algorithms

We evaluated the semi-analytical model GSM (Garver and Siegel, 1997; Maritorena et al., 2002) and the empirical band-ratio algorithm recently proposed to the Arctic Ocean inflow and outflow ecoregions by Lewis and Arrigo (2020) (AOReg.emp). Since remote sensing can only estimate the surface concentration, we computed the chlorophyll-*a* concentration "seen" by a satellite sensor

($[chla]_{sat}$), using discrete samples analysed by HPLC (Morel and Berthon, 1989). $[chla]_{sat}$ is a depth-weighted average for the "penetration depth" (z_{pd}), defined as the first optical depth: $z_{pd} = 1/kd(443)$) (Morel and Berthon, 1989):

$$[chla]_{sat} = \frac{\int_0^{z_{pd}} chla(z)\, e^{-2\, k_d\, z}\, dz}{\int_0^{z_{pd}} e^{-2\, k_d\, z}\, dz} \quad (1)$$

where $chla(z)$ was optically weighted using z and$k_d(443)$ (i.e., $f(chla(z)_{HPLC}, k_d(443))$.

A total of 13 stations from Hudson Bay where both HPLC and C-OPS data were available were used. Figure S1 shows that GSM (r^2: 0.566, $RMSD_{log}$ 0.290, $bias_{log}$: -0.097) reached similar performance of AOReg.emp (r^2: 0.409, $RMSD_{log}$ 0.305, $bias_{log}$: 0.083). These results indicate that both algorithms were slightly biased, but GSM was less scattered than the empirical algorithm. The GSM is more robust in coastal waters (pink symbols) compared to the empirical algorithm that produces very high $[chla]$. Knowing the case-2 nature of the HB, GSM was chosen for this study.

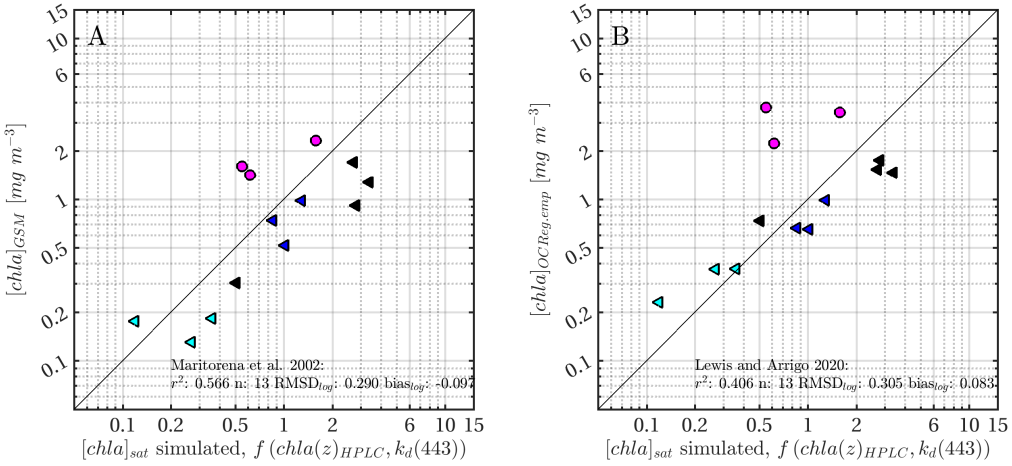

Figure S1. In situ evaluation of satellite-derived chlorophyll-*a* concentration algorithms.

Evaluation of chlorophyll-a concentration ($[chla]_{sat}$, in mg m^{-3}) derived from remote sensing reflectance (R_{rs}, in m^{-1}) using (A) the semi-analytical algorithm (GSM: Maritorena et al., 2002) and (B) the band ratio Arctic Ocean algorithm dedicated to inflow and outflow eco-regions (OCReg.emp: Lewis and Arrigo, 2020). R_{rs} was in-water derived from C-OPS profiles (Mueller et al., 2003). We simulated $[chla]_{sat}$ using coefficient for light attenuaion at 443 nm $k_d(443)$ and profiles of HPLC pigments, similar proposed by Morel and Berthon (1989).

Text S2. Wind direction effect on chlorophyll-*a* concentration

Coastal line orientation is a determinant for water column enrichment forced wind-driven coastal upwelling. The variability of wind directional components can define coastal areas under wind-driven coastal upwelling (Enriquez and Friehe, 1995). In addition to that, the orientation of sea-ice edges (Dumont et al., 2010) can also have similar effect during the sea-ice recovery at the end of the fall-winter transition. However, as illustrated in the Figure S2, relations between time series of $[chla]$, zonal (u) and meridional (v) wind components were difficult to assess in south Hudson Bay centered at $84°$W $57°$N.

Text S3. Water column structure evolution in the South Hudson Bay

Figures S3, S4, S5, S6, S7, and S8 show the water column structure evolution of potential temperature, salinity, stratification, and mixed layer depth, first optical depth, and euphotic zone, time-series of $[chla]$, wind speed and heat flux between 2002 and 2008 (except for 2005) in the South Hudson Bay centered at 84°W 57°N.

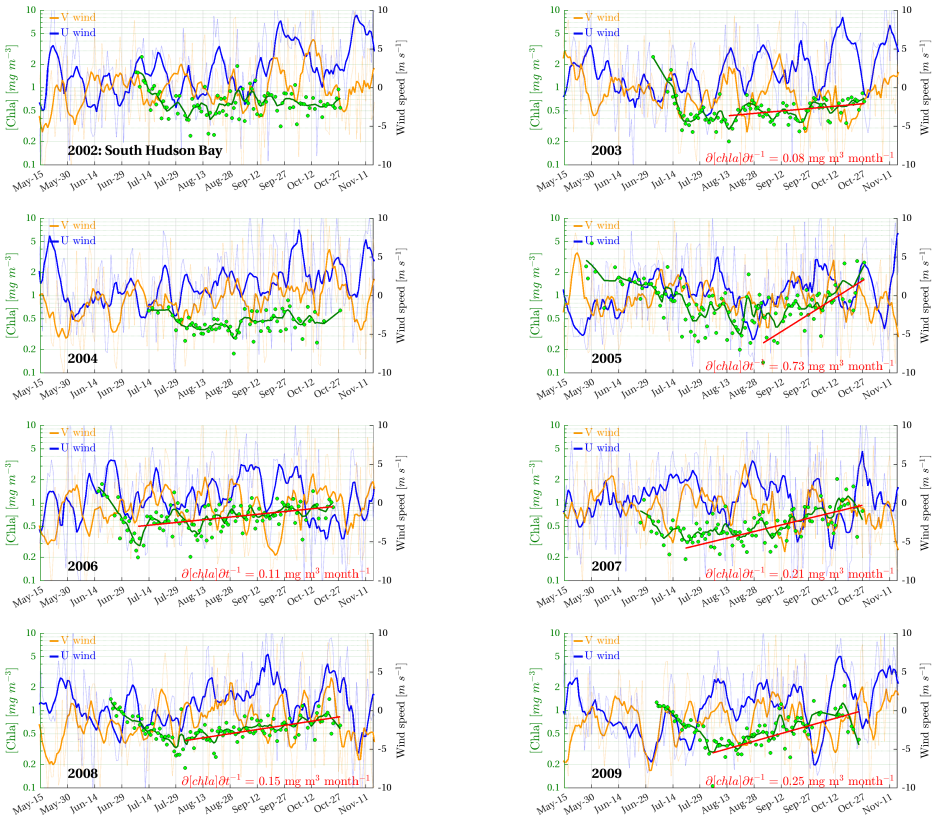

Figure S2. South Hudson Bay: phytoplankton dynamic and wind components.

Time series of chlorophyll-a concentration ($[chla]$: mg m^{-3}, green circles, and 7 days moving average in green line) from the semi-analitical algorithm (GSM: Garver and Siegel, 1997; Maritorena et al., 2002) of Globcolor project, wind u-component (daily in light blue line and 7 days moving average in blue line) and wind v-component (daily in light orange line and 7 days moving average in orange line) from the Canadian Meteorological Centre's Global Deterministic Prediction System Re-Forecasts (CGRF) between 2002 and 2009 in the South Hudson Bay (84°W and 57°N). Chlorophyll-a concentration trends ($\partial\ Chla\,(\partial t)^{-1}$) in the interval of confidence of 99% were plotted between maximum oligotrophic state in summer and fall (red line).

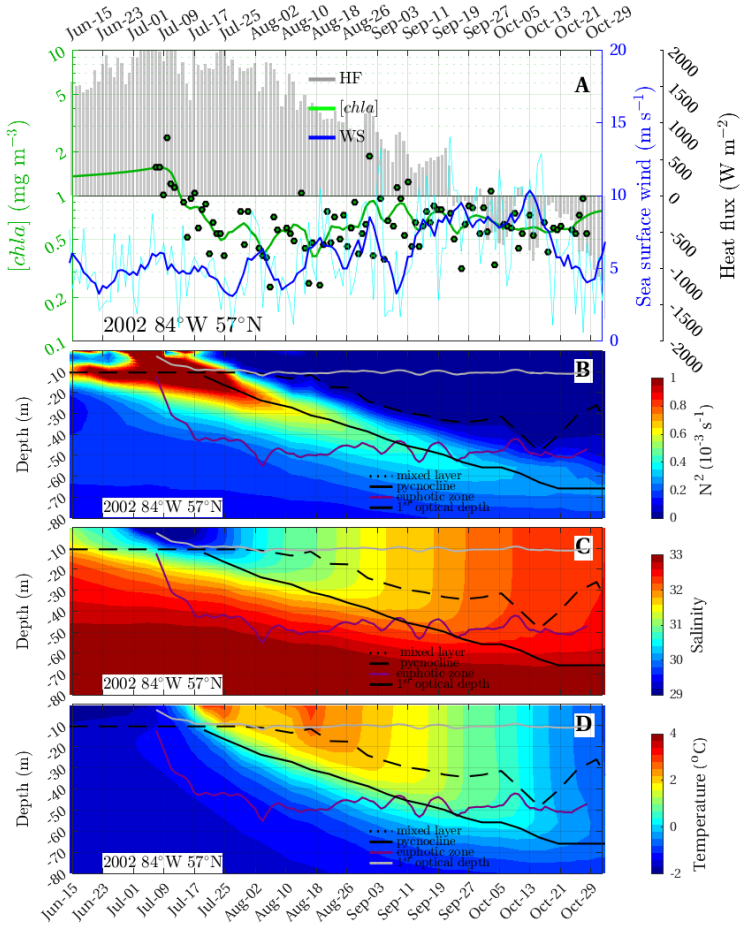

Figure S3. Atmosphere, ocean and phytoplankton, 2002.

Influence of atmospheric forcing and water column structure on phytoplankton phenology: (A) time series of $[chla]$ from Globcolor Project (GSM: Garver and Siegel, 1997; Maritorena et al., 2002) in log scale (daily in green squares, and 7-days movel average in green line), heat flux (HF: grey bars) and wind speed (daily in cyan line, and 7-days movel average in blue line). Profiles in color scale of (B) Brunt-Vaissala frequency (N^2), (C) salinity, and (D) temperature. The vertical profiles had important layer for phytoplankton dynamics marked: satellite-derived first optical depth (z_{OC}: white line) and euphotic depth (z_{eu}: purple line); mixed layer depth (MLD: black traced line); and pycnocline (N^2_{max}: black line).

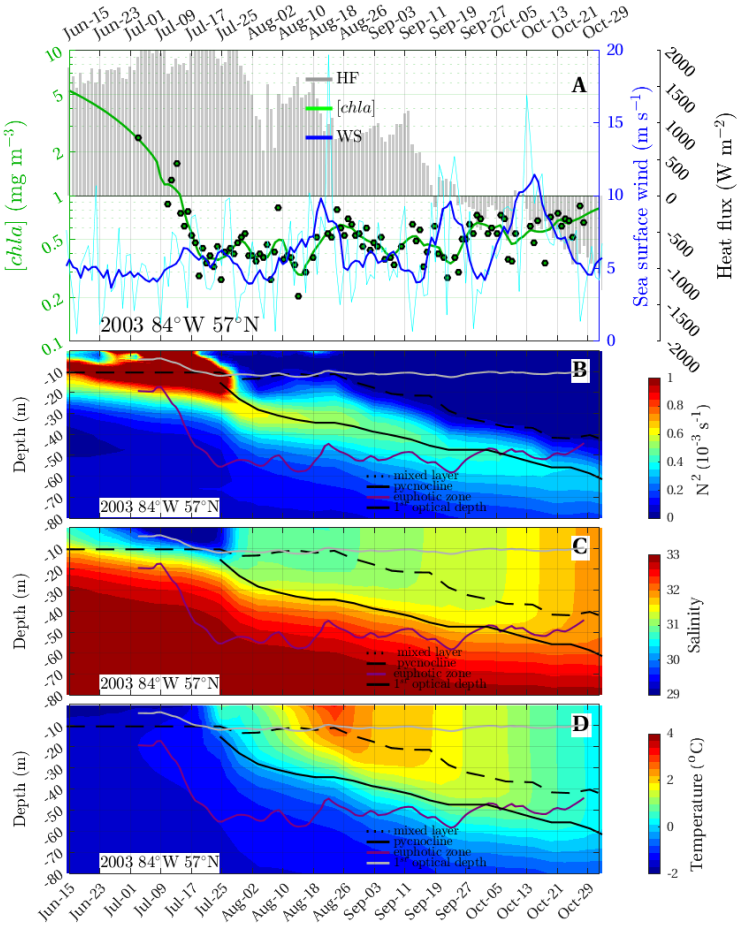

Figure S4. Synergy of the sea-ice model, wind speed reanalysis, and ocean color satellites in south Hudson Bay, 2003.

Influence of atmospheric forcing and water column structure on phytoplankton phenology: (A) time series of $[chla]$ from Globcolor Project (GSM: Garver and Siegel, 1997; Maritorena et al., 2002) in log scale (daily in green squares, and 7-days movel average in green line), heat flux (HF: grey bars) and wind speed (daily in cyan line, and 7-days movel average in blue line). Profiles in color scale of (B) Brunt-Vaissala frequency (N^2), (C) salinity, and (D) temperature. The vertical profiles had important layer for phytoplankton dynamics marked: satellite-derived first optical depth (z_{OC}: white line) and euphotic depth (z_{eu}: purple line); mixed layer depth (MLD: black traced line); and pycnocline (N^2_{max}: black line).

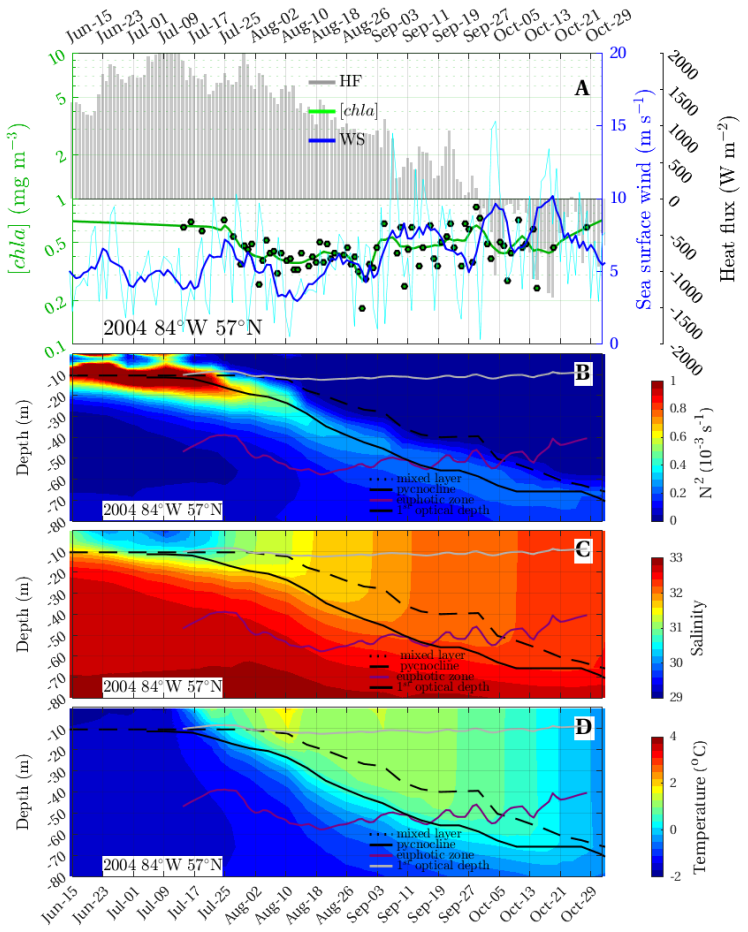

Figure S5. Synergy of the sea-ice model, wind speed reanalysis, and ocean color satellites in South Hudson Bay, 2004.

Influence of atmospheric forcing and water column structure on phytoplankton phenology: (A) time series of $[chla]$ from Globcolor Project (GSM: Garver and Siegel, 1997; Maritorena et al., 2002) in log scale (daily in green squares, and 7-days movel average in green line), heat flux (HF: grey bars) and wind speed (daily in cyan line, and 7-days movel average in blue line). Profiles in color scale of (B) Brunt-Vaissala frequency (N^2), (C) salinity, and (D) temperature. The vertical profiles had important layer for phytoplankton dynamics marked: satellite-derived first optical depth (z_{OC}: white line) and euphotic depth (z_{eu}: purple line); mixed layer depth (MLD: black traced line); and pycnocline (N^2_{max}: black line).

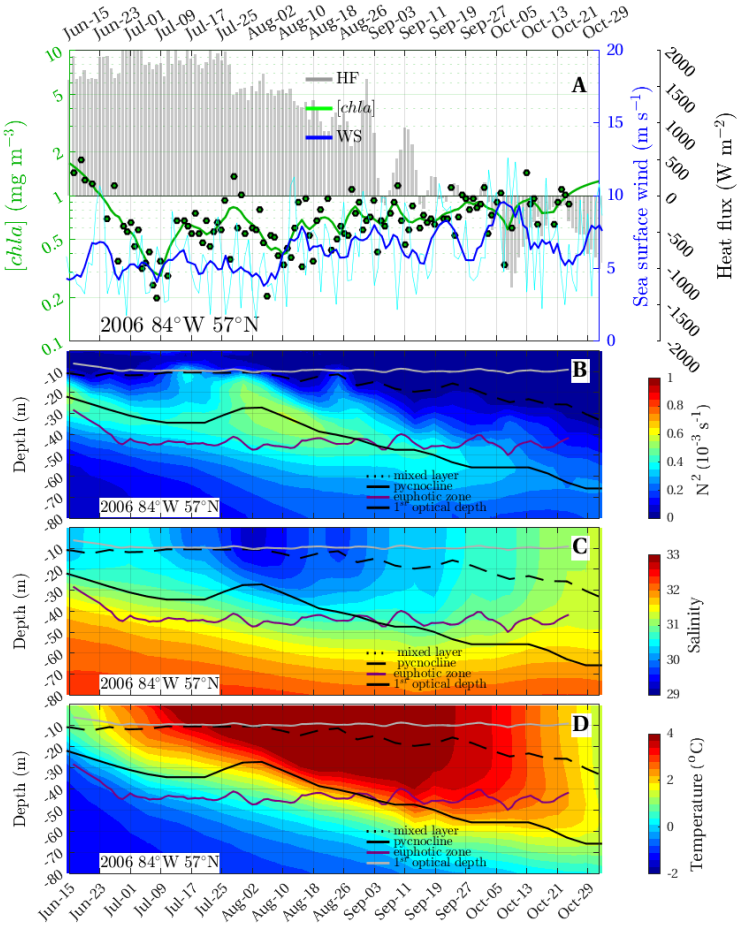

Figure S6. Synergy of the sea-ice model, wind speed reanalysis, and ocean color satellites in South Hudson Bay, 2006.

Influence of atmospheric forcing and water column structure on phytoplankton phenology: (A) time series of $[chla]$ from Globcolor Project (GSM: Garver and Siegel, 1997; Maritorena et al., 2002) in log scale (daily in green squares, and 7-days movel average in green line), heat flux (HF: grey bars) and wind speed (daily in cyan line, and 7-days movel average in blue line). Profiles in color scale of (B) Brunt-Vaissala frequency (N^2), (C) salinity, and (D) temperature. The vertical profiles had important layer for phytoplankton dynamics marked: satellite-derived first optical depth (z_{OC}: white line) and euphotic depth (z_{eu}: purple line); mixed layer depth (MLD: black traced line); and pycnocline (N^2_{max}: black line).

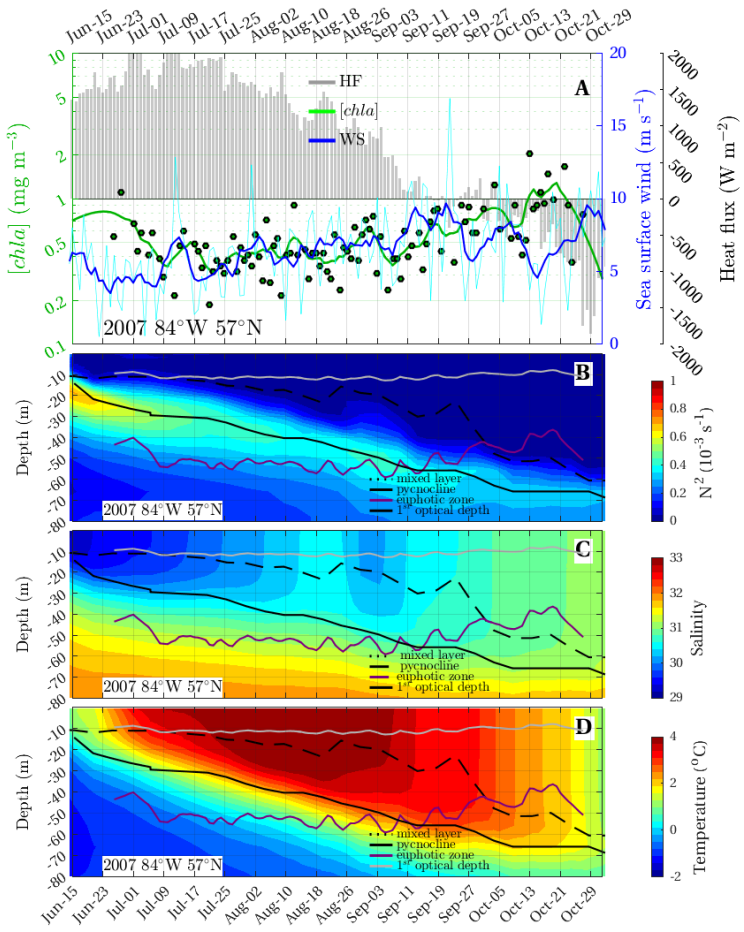

Figure S7. Synergy of the sea-ice model, wind speed reanalysis, and ocean color satellites in South Hudson Bay, 2007.

Influence of atmospheric forcing and water column structure on phytoplankton phenology: (A) time series of $[chla]$ from Globcolor Project (GSM: Garver and Siegel, 1997; Maritorena et al., 2002) in log scale (daily in green squares, and 7-days movel average in green line), heat flux (HF: grey bars) and wind speed (daily in cyan line, and 7-days movel average in blue line). Profiles in color scale of (B) Brunt-Vaissala frequency (N^2), (C) salinity, and (D) temperature. The vertical profiles had important layer for phytoplankton dynamics marked: satellite-derived first optical depth (z_{OC}: white line) and euphotic depth (z_{eu}: purple line); mixed layer depth (MLD: black traced line); and pycnocline (N^2_{max}: black line).

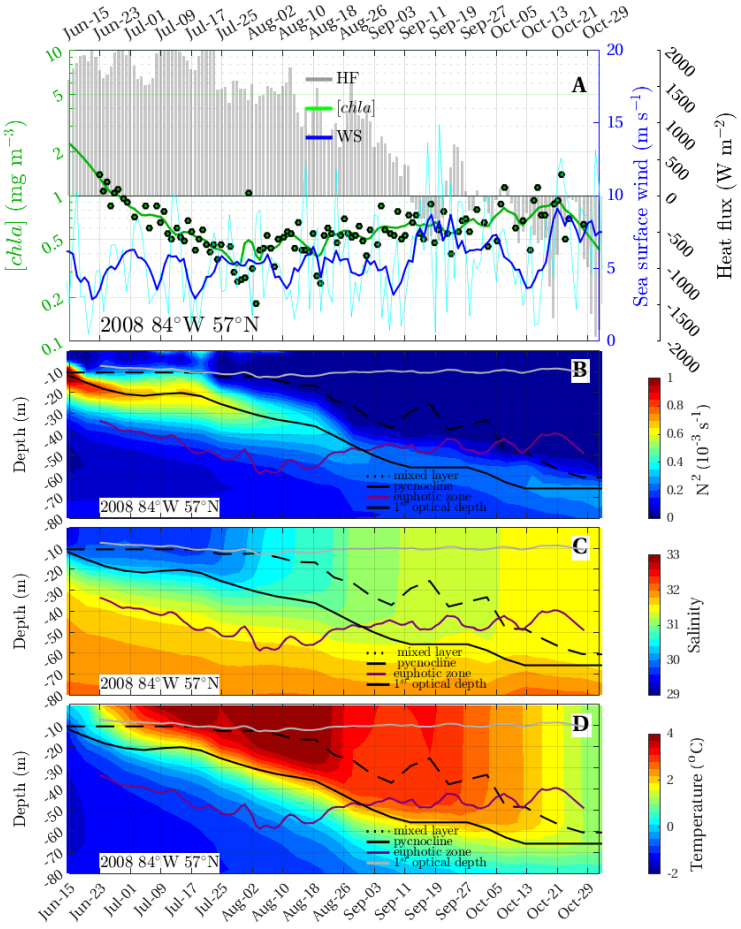

Figure S8. Synergy of the sea-ice model, wind speed reanalysis, and ocean color satellites in South Hudson Bay, 2008.

Influence of atmospheric forcing and water column structure on phytoplankton phenology: (A) time series of $[chla]$ from Globcolor Project (GSM: Garver and Siegel, 1997; Maritorena et al., 2002) in log scale (daily in green squares, and 7-days movel average in green line), heat flux (HF: grey bars) and wind speed (daily in cyan line, and 7-days movel average in blue line). Profiles in color scale of (B) Brunt-Vaissala frequency (N^2), (C) salinity, and (D) temperature. The vertical profiles had important layer for phytoplankton dynamics marked: satellite-derived first optical depth (z_{OC}: white line) and euphotic depth (z_{eu}: purple line); mixed layer depth (MLD: black traced line); and pycnocline (N^2_{max}: black line).

Text S4. Seasonal phytoplankton photo-acclimation

Nonparametric one-way analysis of variance and multi-statistic tests (MatLab functions: anova1.m and multcompare.m) of $b_{bp}(\lambda)$ and $[chla]$ indicated that phytoplankton communities and bio-optics characteristics are significant are distinct between each months with a confidence interval of 95% ($P < 0.05$). Figure S9 show satellite derived monthly climatologies of $[chla]$, C_{phy}, C_{phy}:$[chla]$ ratio, $b_{bp}(555)$, $b^k_{bp}(555)$, and $b^k_{bp}(555)$:$b_{bp}(555)$ ratio obtained from 1998 to 2018 in the Hudson Bay System. The Figure S10 shows monthly maps of satellite derived climatology of $b^k_{bp}(555)$:$b_{bp}(555)$ ratio.

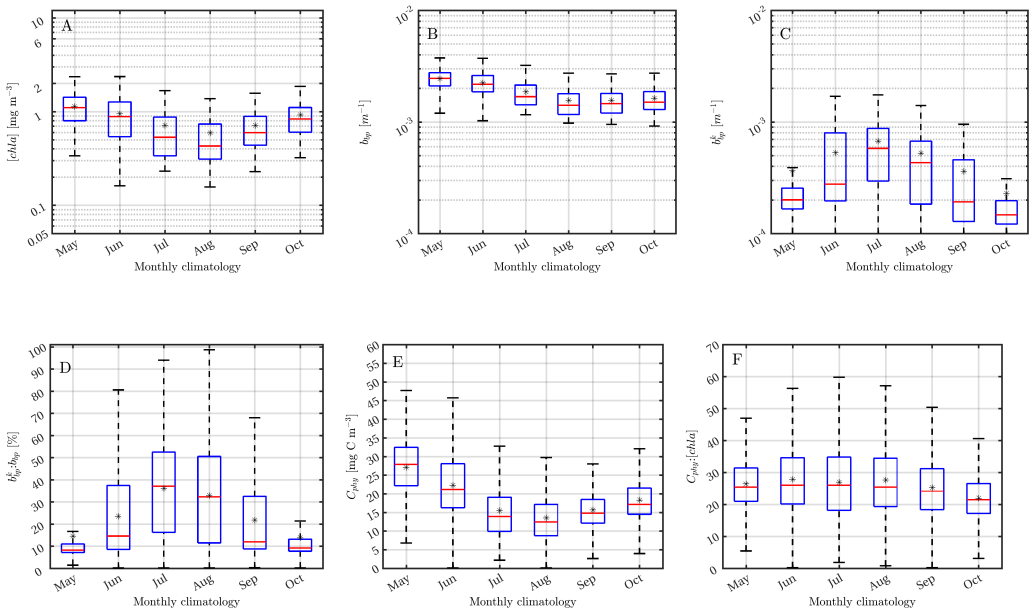

Figure S9. Seasonal influence of bio-optical properties in the Hudson Bay.

Boxplots of satellite ocean color monthly climatology (May, June, July, August, September, and October) of (A) chlorophyll-a concentration ($[chla]$), (D) backscattering coefficient at 555 nm ($b_{bp}(55)$), (c) non-algal particle backgorund contribution to backscattering at 555 nm ($b^k_{bp}(555)$), (d) relative contribution of NAP backgroung to particle backscattering coefficient ($b^k_{bp}(555)/b_{bp}(555)$: in %), (E) phytoplankton carbon (C_{phy}), and (F) ratio phytoplankton carbon to chlorophyll (C_{phy}:$[chla]$) obtained between 1998 and 2018. Satellite-derived products were calculated using the semianalytical algorithm (GSM: Garver and Siegel, 1997; Maritorena et al., 2002) of the Globcolor Project merged daily 4 km products. The central red line marks are respective median, black ashes are averages, the edges of the blue boxes are the 25^{th} and 75^{th} percentiles, the whiskers extend to the most extreme data points between $\pm 0.26\sigma$ considering a normal distribution.

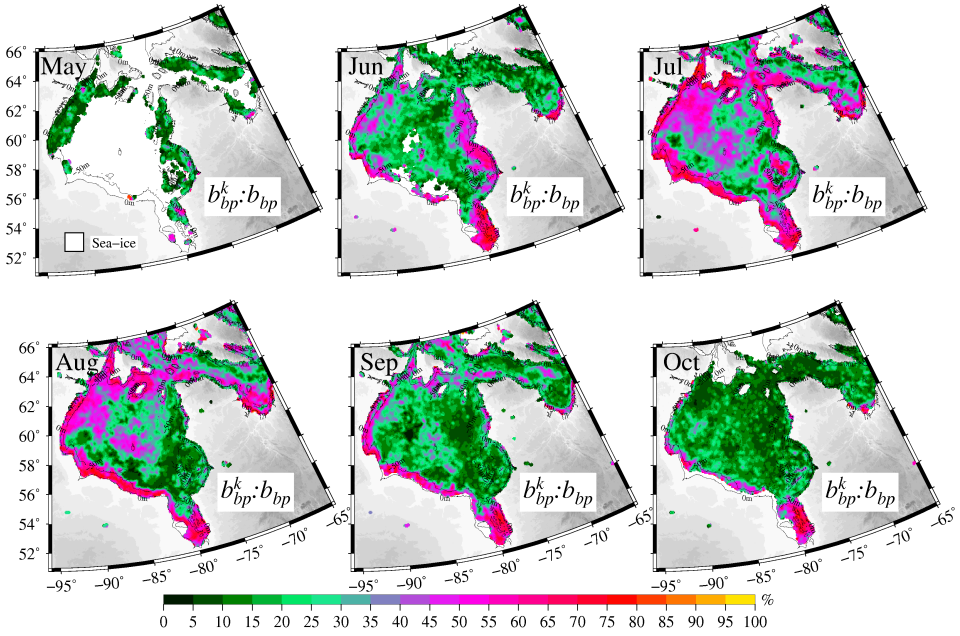

Figure S10. Seasonal influence of non-algal particles on light backscattering coefficient.

Satellite ocean color monthly climatology (May, June, July, August, September, and October) relative contribution of NAP to particle backscattering coefficient ($b_{bp}^k(555)/b_{bp}(555)$: in $\%$) obtained between 1998 and 2018. $b_{bp}^k(555)$ were estimated using satellite-derived $b_{bp}(555)$ and $[chla]$ calculated from the semi-analytical algorithm (GSM: Garver and Siegel, 1997; Maritorena et al., 2002) of the Globcolor Project merged daily 4 km products.

References

Dumont D, Gratton Y, Arbetter TE. 2010. Modeling wind-driven circulation and landfast ice-edge processes during polynya events in northern Baffin Bay. *Journal of Physical Oceanography* **40**(6): 1356–1372. ISSN 0022-3670. doi: 10.1175/2010JPO4292.1.

Enriquez AG, Friehe CA. 1995. Effects of wind stress and wind stress curl variability on coastal Upwelling. *Journal of Physical Oceanography* **25**: 1651–1671. ISSN 0022-3670. doi:10.1175/1520-0485(1995)025⟨1651:EOWSAW⟩2.0.CO;2.

Garver SA, Siegel DA. 1997. Inherent optical property inversion of ocean color spectra and its biogeochemical interpretation, 1. Time series from the Sargasso Sea. *Journal of Geophysical Research* **102**(96): 18607–18625. doi: 10.1029/96JC03243.

Lewis KM, Arrigo KR. 2020. Ocean Color Algorithms for Estimating Chlorophyll-*a* , CDOM Absorption, and Particle Backscattering in the Arctic Ocean. *Journal of Geophysical Research: Oceans* **125**(6): 1–23. doi: 10.1029/2019jc015706.

Maritorena S, Siegel DA, Peterson AR. 2002. Optimization of a semianalytical ocean color model for global-scale applications. *Applied optics* **41**(15):

2705–2714. doi:10.1364/AO.41.002705.

Morel A, Berthon JF. 1989. Surface pigments, algal biomass profiles, and potential production of the euphotic layer: Relationships reinvestigated in view of remote-sensing applications. *Limnology and Oceanography* **34**(8): 1545–1562. doi:10.4319/lo.1989.34.8.1545.

Mueller JL, Fargion GS, Mcclain CR, Morel A, Frouin R, Davis C, Arnone R, Carder K, Steward RG, Hooker S, Mobley CD, Mclean S, Holben B, Pietras C, Knobelspiesse KD, Porter J. 2003. Ocean Optics Protocols For Satellite Ocean Color Sensor Validation, Revision 4. Volume III: Radiometric Measurements and Data Analysis Protocols. NASA.